Appendix S1. Detailed description of the water balance model

S1.1. Model overview

The model calculates water balance on a daily step basis for a given forest stand and for the period corresponding to daily precipitation, temperature and net radiation data. It follows the design principles of SIERRA (Mouillot et al., 2001; Ruffault et al., 2014, 2013) and BILJOU (Granier et al., 2007, 1999), although some features are taken from Prentice et al. (1993).

S1.1.1 Soil state variables

The soil of the stand is described using three layers (topsoil: 0 – 30 cm; subsoil: from 30 cm to soil depth; rocky layer: from soil depth to 400 cm). Soil texture (i.e. percent of sand, silt and clay), bulk density and rock fragment content can differ between topsoil and subsoil. Although this feature was not used in our study, the model allows specifying a rocky layer because Mediterranean plants may extend their roots into cracks existing in the parent rock; it has the same texture as the subsoil (but 95% of rocks) (Ruffault et al., 2013). The *soil depth* attribute refers to the sum of topsoil and subsoil layers (thus, subsoil may not exist in very shallow soils). Relative soil moisture content is tracked at each layer using $W = \theta_\Psi / \theta_{fc}$, the proportion of soil moisture θ_Ψ in relation to field capacity θ_{fc}. Following Reynolds et al. (2000), soil moisture θ_Ψ corresponding to a given water potential Ψ is calculated using the pedotransfer functions of Saxton et al. (1986):

$$\theta_\Psi = (-\Psi/A)^{1/B} \quad (1)$$

$$A = 100 \cdot \exp[-4.396 - 0.0715 \cdot P_{clay} - 0.0004880 \cdot P_{sand}^2 - 0.00004285 \cdot P_{sand}^2 \cdot P_{clay}]$$

$$B = -3.140 - 0.00222 \cdot P_{clay}^2 - 0.00003484 \cdot P_{sand}^2 \cdot P_{clay}$$

where and P_{clay} and P_{sand} are the percentage of clay and sand, respectively. Soil water holding capacity (in mm) in a given soil layer is:

$$VolMax = d \cdot (1 - P_{rocks}) \cdot q_{fc} \quad (2)$$

where d is the depth of the soil layer (in mm) and P_{rocks} is the rock fragment content.

S1.1.2 Vegetation state variables

Vegetation is described using a set of plant cohorts. Each plant cohort is defined by species identity (*sp*), height (*h*, in cm), depth of rooting system (*z*, in mm) and leaf area index (*LAI*, one-side leaf area of plants in the cohort per surface area of the stand). The total *LAI* of the stand is the sum of cohort *LAI* values. The rooting system of plants is described by the linear dose response model (Collins and Bras, 2007; Schenk and Jackson, 2002) as follows (see Fig. S1.1):

$$Y(z) = \frac{1}{1+(z/D_{50})^c} \tag{3}$$

where Y is the cumulative fraction of total root mass between surface and depth z; D_{50} is the depth above which 50% of the root mas is located; and c is a shape parameter related to D_{50} and D_{95} as $c = 2.94 / \ln(D_{50} / D_{95})$.

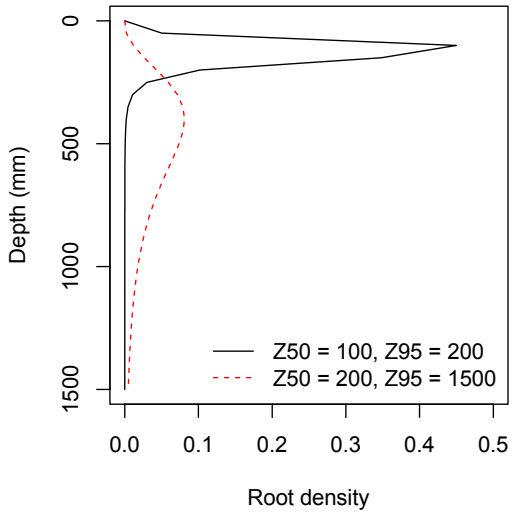

Fig. S1.1: Two examples of root density profile according to the linear dose response model.

The depth of soil layers and the linear dose response model is used to determine $v_{i,s}$, the proportion of plant fine roots of cohort *i* that are in a given soil layer *s*. The minor fraction of mass located below soil depth is redistributed within the existing layers and the proportion of roots in each soil layer is assumed proportional to the amount of water extracted from it. All vegetation variables except *LAI* (for deciduous species) are assumed to stay constant during water balance simulations.

S1.1.3 Water balance process scheduling

Every day the model first updates leaf area values according to the phenology of species and calculates light extinction. After that, the model updates soil water content of soil layers in

two steps: (1) it increases soil moisture due to precipitation, P, after accounting for canopy interception loss, I, surface runoff, R, and deep drainage, D; (2) it decreases water content due to bare soil evaporation, E, and plant transpiration, T. Daily variations in soil water content can be summarized as:

$$\Delta SWC = P - I - R - D - E - T \quad (4)$$

After updating soil layers, the model determines drought stress of each plant cohort, according to whole-plant relative water conductance.

S1.2. Details of processes

S1.2.1 Leaf phenology

Plant species can have either evergreen or winter deciduous phenology. Evergreen plants maintain constant leaf area over the year, whereas in deciduous plants leaf-phenological status is updated daily, represented by ϕ_i, the fraction of maximum leaf area. Leaf area index (LAI) values of deciduous plants are adjusted for leaf phenology following (Prentice et al., 1993; Sitch et al., 2003):

$$LAI_i^f = LAI_i \cdot f_i \quad (5)$$

Budburst occurs when daily temperature exceeds 5ºC and ϕ_i increases linearly from 0 to 1 as function of the degree days above 5ºC, until a species-specific value S_{GDD} is reached. In autumn, ϕ_i becomes 0 when average daily temperature falls again below 5ºC (Sitch et al., 2003).

S1.2.2 Light extinction

Light extinction is used to modulate the evaporative demand for plant cohorts in the shade and to determine the amount of light reaching the ground. The proportion of light available after removing the light intercepted by a single plant cohort i of species sp follows Beer-Lambert's light extinction equation:

$$L = e^{-k_{sp} \times LAI_i^f} \quad (6)$$

where k_{sp} is the extinction coefficient of species sp. To calculate the proportion of light available for a given plant cohort one must accumulate the light extinction caused by cohorts whose crown is above that of the target cohort:

$$L_i = e^{-\sum_j k_{sp(j)} \cdot LAI_j^f \cdot p_{ij}} \quad (7)$$

where $sp(j)$ is the species of cohort j. Because plant cohorts may differ in height only slightly, the adjusted leaf area is multiplied by p_{ij}, the proportion of the crown of cohort j that overtops that of cohort i:

$$p_{ij} = \max(0, \min(1, (h_j - h_i) / (h_j - h_j \cdot b_{sp(j)})) \quad (8)$$

where $b_{sp(j)}$ is the species-specific proportion of total plant height that corresponds to the crown. In other terms, cohorts whose crown is completely above that of i reduce the amount of light available more strongly by than cohorts that are only slightly taller. L_{ground}, the proportion of radiation that reaches the ground, is calculated as:

$$L_{ground} = e^{-\sum_i k_{sp} \cdot LAI_i^f} \quad (9)$$

S1.2.3 Rainfall interception loss

Rainfall interception loss, I, is modelled following the Gash et al. (1995) analytical interception model for sparse canopies, where rain is assumed to fall in a single event during the day. First, the amount of rainfall needed to saturate the canopy is calculated:

$$P_G = -\frac{S/C}{ER} \cdot \ln(1 - ER) \quad (10)$$

where S is the canopy water storage capacity (in mm) – i.e. the minimum amount of water needed to saturate the canopy –, C is the canopy cover and ER is the ratio of evaporation rate to rainfall rate during the rainfall event. The amount of water evaporated from interception, I (mm), is calculated as:

$$\begin{aligned} I &= C \cdot P_G + C \cdot ER \cdot (P - P_G) \quad \text{if } P > P_G \\ I &= C \cdot P \quad \text{if } P \leq P_G \end{aligned} \quad (11)$$

where P is the daily gross precipitation (in mm). Net rainfall, P_{net}, is calculated as the difference between gross rainfall and interception loss. Although interception models are normally applied to single-canopy stands, we apply the sparse Gash model to the whole stand (including shrubs). Moreover, in our implementation stem interception is lumped with canopy interception, so that S represents both. Following Watanabe & Mizutani (1996) we estimate S from adjusted LAI values:

$$S = \sum_i s_{sp} \cdot LAI_i^f \tag{12}$$

where s_{sp} is the depth of water that can be retained by leaves and trunks of a particular species per unit of leaf area index (mm·LAI^{-1}). To estimate the stand cover, C, we use the complement of the percentage of light that reaches the ground, i.e. $C = 1 - L_{ground}$ (Deguchi et al., 2006). Fig. S1.2 shows examples of relative throughfall, calculated according to the interception model, under different situations.

S1.2.4 Runoff

Runoff, R (in mm), is calculated using the USDA SCS curve number method, as in Boughton (1989):

$$R = \frac{(P_{net} - 0.2 \cdot V_{soil})^2}{(P_{net} - 0.8 \cdot V_{soil})} \tag{13}$$

where V_{soil} (in mm) is the overall soil water retention capacity (i.e. the sum of *VolMax* of topsoil and subsoil).

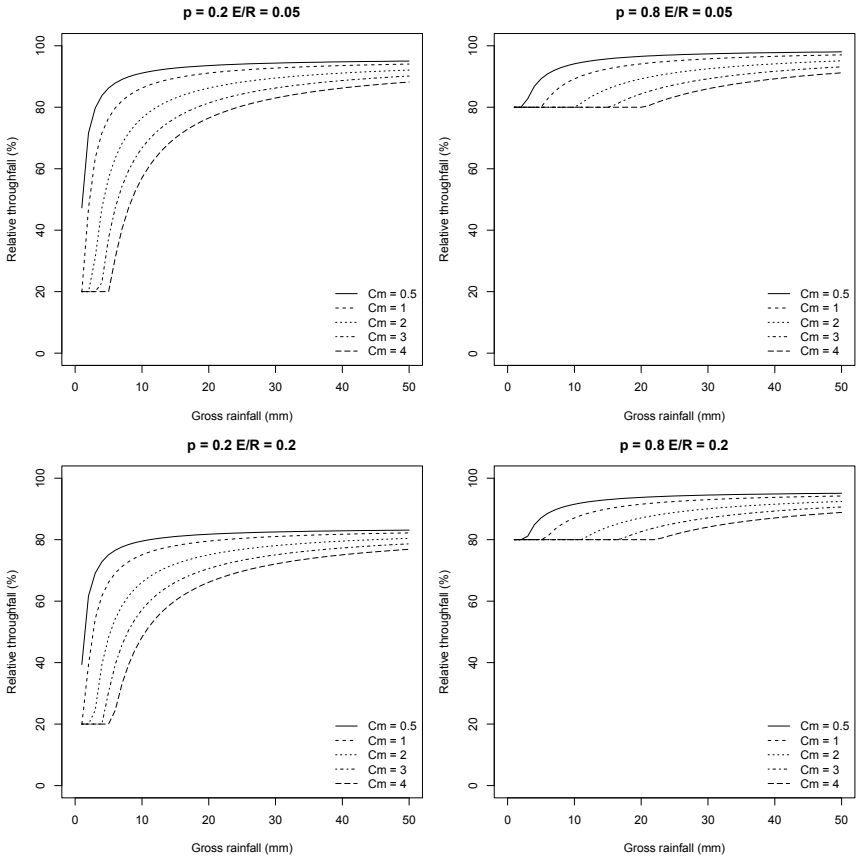

Fig. S1.2: Examples of canopy interception with different *Cm* (canopy water storage capacity; *Cm* = *S*), *E/R* (ratio between evaporation and rainfall rates) and *p* (throughfall coefficient; *p* = 1 – *C*).

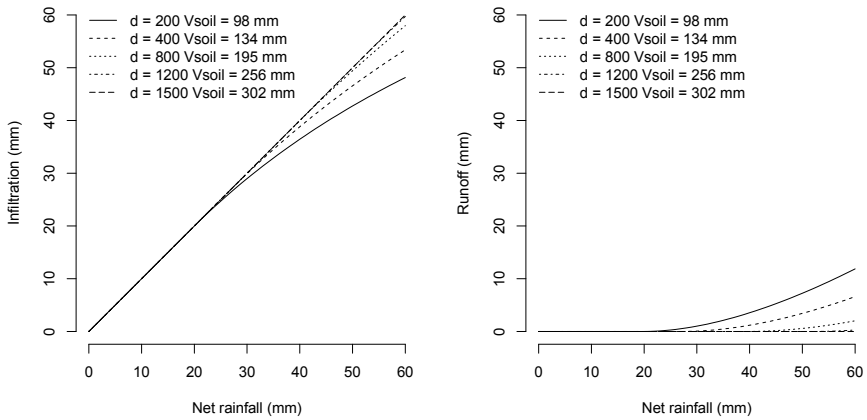

Fig. S1.3: Examples of infiltration/runoff calculation for different values of net rainfall and overall retention capacity, V_{soil}, calculated from different soil depths (topsoil+subsoil), *d*, and assuming that soil texture is 15% clay and 25% sand. Rock fragment content was 25% and 40% for the topsoil and subsoil, respectively.

S1.2.5 Infiltration and percolation

The amount of water infiltrating into the soil is $P_{net} - R$. Following Granier (1999), part of the water reaching one soil layer percolates quickly through the macropores. The remaining water is retained by the micropores refilling the current soil layer. When this soil layer reaches its field capacity the excess of water percolates to the soil layer below. The water percolating from the lowest layer is considered deep drainage, *D*. Macroporosity values are calculated for each soil layer from its percentage of sand and bulk density, using the equations given in Stolf et al. (2011).

S1.2.6 Potential evapotranspiration

Daily potential evapotranspiration, *PET* (in $mm \cdot day^{-1}$), is calculated following Prentice et al. (1993) who argued that, on the basis of the theory of equilibrium evapotranspiration (Jarvis and McNaughton, 1986), a water demand function suitable for landscape applications was:

$$PET = \left(\frac{s}{s+\gamma}\right)\frac{R_n}{\lambda} \tag{14}$$

where R_n is the net radiation – in our case the daily net radiation (in $J \cdot m^{-2} \cdot day^{-1}$) –, σ is the slope of the saturated vapor pressure (in $Pa \cdot K^{-1}$), $\gamma = 65$ $Pa \cdot K^{-1}$ is the psychrometer constant and $\lambda = 2.5 \cdot 10^6$ $J \cdot kg^{-1}$ is the latent heat vaporization of water. Following Prentice et al. (1993), we used $\sigma = 2.503 \cdot 10^6 \cdot \exp(17.269 \cdot T/(237.3+T))/(237.3+T)^2$ but neglected the weak dependence of γ and λ on temperature. Daily net radiation (in $J \cdot m^{-2} \cdot day^{-1}$) is estimated from solar radiation (R_s) and temperature using (Linacre, 1968):

$$R_n = (1 - a) \cdot R_s - 1927.987 \cdot (1+4 \cdot nN) \cdot (100 - T) \tag{15}$$

where α is the surface albedo (by default, $\alpha = 0.17$) and nN is the proportion of bright sun hours during daylight (by default, $nN = 0.25$ in rainy days and $nN = 0.75$ in non-rainy days).

S1.2.7 Bare soil evaporation

Evaporation from the soil surface is modeled as in Mouillot et al. (2001), who followed Ritchie (1972). First, the model determines the time needed to evaporate the current water deficit (difference between field capacity and current moisture) in the surface soil layer:

$$t = \left(\frac{MaxVol_1 \cdot (1 - W_1)}{g}\right)^2 \tag{16}$$

where γ is the maximum daily evaporation ($mm \cdot day^{-1}$). The calculated time is used to determine the 'supplied' evaporation, S_{soil}:

$$S_{soil} = g \cdot (\sqrt{t+1} - \sqrt{t}) \tag{17}$$

The amount of water evaporated from the soil, E_{soil}, is then calculated as the minimum between supply and demand (Federer, 1982), the latter being the product of PET and the proportion of light that reaches the ground:

$$E_{soil} = \min(PET \cdot L_{ground}, S_{soil}) \tag{18}$$

Finally, E_{soil} is distributed along the soil profile according to an exponential decay function with an extinction coefficient κ (Mouillot et al., 2001).

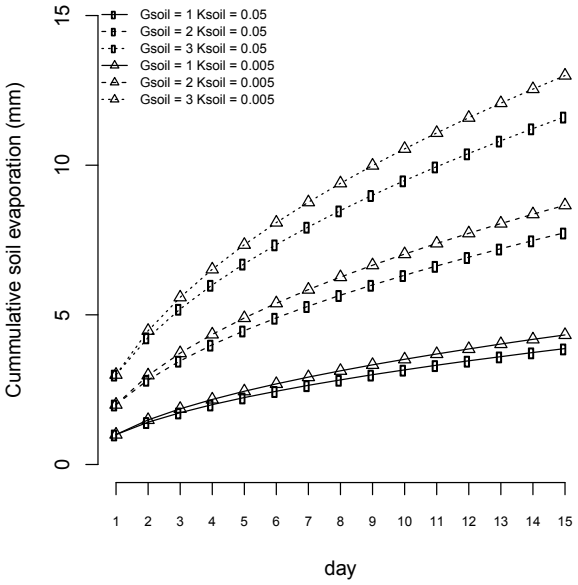

Fig. S1.4: Cumulative bare soil evaporation for different values of maximum evaporation rate γ and extinction coefficient κ. Three soil layers (0 – 30 cm; 30 – 150 cm; 150 – 400 cm) are initialized at field capacity ($MaxVol_1$ = 50 mm; $MaxVol_2$ = 201 mm; $MaxVol_3$ = 35 mm). L_{ground} was 100% and *PET* was assumed not to be limiting. When the extinction coefficient is smaller a higher proportion of the evaporated water is removed from the subsoil and less from the topsoil. This causes more water being available to calculate *t* in the next step.

S1.2.8 Plant transpiration

Maximum transpiration of the forest stand assuming no water limitations, T_{max}, is a function of *PET* and LAI_c – the cumulative leaf area of the forest stand –, according to the experimental equation given in Granier et al. (1999):

$$\frac{T_{\max}}{PET} = -0.006 \cdot LAI_c^2 + 0.134 \cdot LAI_c + 0.036 \quad (19)$$

Eq. 19 has already been adopted for Mediterranean biomes (Fyllas and Troumbis, 2009; Ruffault et al., 2013).

Actual plant transpiration is calculated for each soil layer separately. For each plant cohort *i* and soil layer *s*, the model first estimates the a whole-plant relative water conductance, $K_{i,s}$, which varies between 0 and 1 depending on Ψ_{sp}, the species-specific potential at which conductance is 50% of maximum, and Ψ_s, the water potential in layer *s*.

$$K_{i,s} = \exp\left(-\ln(0.5) \cdot \frac{\Psi_s}{\Psi_{sp}}\right) \quad (20)$$

where r is an exponent that modulates the steepness of the decrease in relative conductance when soil potential becomes negative (by default, $r = 3$) and ln(0.5) is used to ensure that $K_{i,s}$ (Ψ_{sp}) = 0.5 (Fig. S1.5).

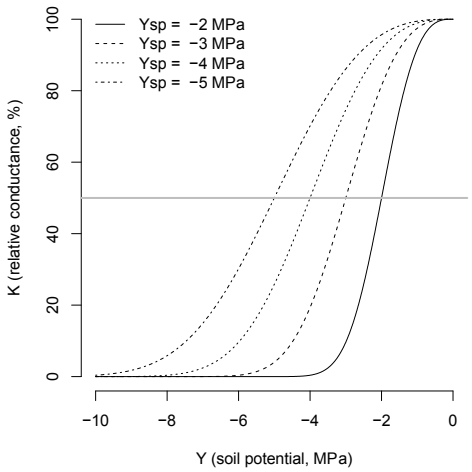

Fig. S1.5: Whole-plant relative water conductance functions for different Ψ_{sp} values (r = 3 in all cases).

Actual transpiration of plant cohort i from a given soil layer s, $T_{i,s}$, is defined as the product of (Mouillot et al., 2001): (i) the maximum transpiration of the stand, T_{max}, calculated using eq. 19; (ii) the proportion of T_{max} that corresponds to the plant cohort, calculated on the basis of its leaf area and the amount of light available to it, L_i; (iii) the relative whole-plant conductance, $K_{i,s}$, corresponding to the species and water potential in layer s; (iv) the proportion of plant fine roots in layer s, $v_{i,s}$:

$$T_{i,s} = T_{max} \cdot \frac{L_i \cdot LAI_i^f}{\sum_j L_j \cdot LAI_j^f} \cdot K_{i,s} \cdot v_{i,s} \quad (21)$$

The total amount of water transpired by plants, T, is the sum of $T_{i,s}$ values over all plant cohorts and soil layers. Assuming no water limitations (i.e. $K_{i,s} = 1$), we have that maximum stand transpiration is achieved:

$$T = \sum_s \sum_i T_{i,s} = \underset{(K_{i,s}=1)}{\ldots} = T_{max} \quad (22)$$

Total stand transpiration will be lower than T_{max} if soil water potential in any layer is negative enough to cause a significant reduction in whole-plant conductance. At the plant level, the transpiration of a given plant cohort will be lower than that of others if: (1) the cohort is under

the shade; (2) the cohort has a lower amount of leaf area; (3) the soil layers exploited by the cohort have more negative water potentials.

S1.3 Plant daily drought stress

Similarly to Mouillot et al. (2002), daily drought stress of a given plant cohort *i*, DDS_i, is defined as the complement of relative whole-plant conductance and is aggregated across soil layers using the proportion of fine roots in each layer as weights:

$$DDS_i = f_i \cdot \sum_s (1 - K_{i,s}) \cdot v_{i,s} \quad (23)$$

Leaf-phenological status is included in eq. 23 to prevent winter deciduous plants from suffering drought stress during winter. Daily drought stress values can be later used to define drought stress indices for larger temporal scales, as presented in the main text.

References

Collins, D.B.G., Bras, R.L., 2007. Plant rooting strategies in water-limited ecosystems. Water Resour. Res. 43, W06407. doi:10.1029/2006WR005541

Deguchi, A., Hattori, S., Park, H.-T., 2006. The influence of seasonal changes in canopy structure on interception loss: Application of the revised Gash model. J. Hydrol. 318, 80–102. doi:10.1016/j.jhydrol.2005.06.005

Federer, C., 1982. Transpirational supply and demand: plant, soil, and atmospheric effects evaluated by simulation. Water Resour. Res. 18, 355–362.

Fyllas, N.M., Troumbis, A.Y., 2009. Simulating vegetation shifts in north-eastern Mediterranean mountain forests under climatic change scenarios. Glob. Ecol. Biogeogr. 18, 64–77. doi:10.1111/j.1466-8238.2008.00419.x

Gash, J., Lloyd, C., Lachaud, G., 1995. Estimating sparse forest rainfall interception with an analytical model. J. Hydrol. 170.

Granier, A., Bréda, N., Biron, P., Villette, S., 1999. A lumped water balance model to evaluate duration and intensity of drought constraints in forest stands. Ecol. Modell. 116, 269–283.

Granier, A., Reichstein, M., Bréda, N., Janssens, I.A., Falge, E., Ciais, P., Grünwald, T., Aubinet, M., Berbigier, P., Bernhofer, C., Buchmann, N., Facini, O., Grassi, G., Heinesch, B., Ilvesniemi, H., Keronen, P., Knohl, A., Köstner, B., Lagergren, F., Lindroth, A., Longdoz, B., Loustau, D., Mateus, J., Montagnani, L., Nys, C., Moors, E., Papale, D., Peiffer, M., Pilegaard, K., Pita, G., Pumpanen, J., Rambal, S., Rebmann, C.,

Rodrigues, A., Seufert, G., Tenhunen, J., Vesala, T., Wang, Q., 2007. Evidence for soil water control on carbon and water dynamics in European forests during the extremely dry year: 2003. Agric. For. Meteorol. 143, 123–145. doi:10.1016/j.agrformet.2006.12.004

Jarvis, P., McNaughton, K., 1986. Stomatal control of transpiration: Scaling Up from leaf to region. Adv. Ecol. Res. 15, 1–49.

Linacre, E.T., 1968. Estimating the net-radiation flux. Agric. Meteorol. 93, 49–63.

Mouillot, F., Rambal, S., Joffre, R., 2002. Simulating climate change impacts on fire frequency and vegetation dynamics in a Mediterranean-type ecosystem. Glob. Chang. Biol. 8, 423–437.

Mouillot, F., Rambal, S., Lavorel, S., 2001. A generic process-based SImulator for meditERRanean landscApes (SIERRA): design and validation exercises. For. Ecol. Manage. 147, 75–97. doi:10.1016/S0378-1127(00)00432-1

Prentice, I.C., Sykes, M.T., Cramer, W., 1993. A simulation model for the transient effects of climate change on forest landscapes. Ecol. Modell. 65, 51–70. doi:10.1016/0304-3800(93)90126-D

Reynolds, C.A., Jackson, T.J., Rawls, W.J., 2000. Estimating soil water-holding capacities by linking the Food and Agriculture Organization Soil map of the world with global pedon databases and continuous pedotransfer functions. Water Resour. Res. 36, 3653–3662. doi:10.1029/2000WR900130

Ritchie, J., 1972. Model for predicting evaporation from a row crop with incomplete cover. Water Resour. Res. 8, 1204–1213.

Ruffault, J., Martin-StPaul, N.K., Duffet, C., Goge, F., Mouillot, F., 2014. Projecting future drought in Mediterranean forests: bias correction of climate models matters! Theor. Appl. Climatol. 117, 113–122. doi:10.1007/s00704-013-0992-z

Ruffault, J., Martin-StPaul, N.K., Rambal, S., Mouillot, F., 2013. Differential regional responses in drought length, intensity and timing to recent climate changes in a Mediterranean forested ecosystem. Clim. Change 117, 103–117. doi:10.1007/s10584-012-0559-5

Saxton, K.E., Rawls, W.J., Romberger, J.S., Papendick, R.I., 1986. Estimating generalized soil-water characteristics from texture. Soil Sci. Soc. Am. J. 50, 1031–1036.

Schenk, H., Jackson, R., 2002. The global biogeography of roots. Ecol. Monogr. 72, 311–328.

Sitch, S., Smith, B., Prentice, I.C., Arneth, a., Bondeau, a., Cramer, W., Kaplan, J.O., Levis, S., Lucht, W., Sykes, M.T., Thonicke, K., Venevsky, S., 2003. Evaluation of ecosystem dynamics, plant geography and terrestrial carbon cycling in the LPJ dynamic global vegetation model. Glob. Chang. Biol. 9, 161–185. doi:10.1046/j.1365-2486.2003.00569.x

Stolf, R., Thurler, Á., Oliveira, O., Bacchi, S., Reichardt, K., 2011. Method to estimate soil macroporosity and microporosity based on sand content and bulk density. Rev. Bras. Ciencias do Solo 35, 447–459.

Watanabe, T., Mizutani, K., 1996. Model study on micrometeorological aspects of rainfall interception over an evergreen broad-leaved. Agric. For. Meteorol. 80, 195–214.

Appendix S2. Model sensitivity analyses

S2.1 Analyses

We conducted sensitivity analyses to determine which model parameters were critically driving model's predictions. The baseline parameterization was the following:

Climate – In the baseline scenario, annual rainfall was 622 mm and annual PET was 1211 mm (Fig. S2.1.a).

Soil – Soil was set to 100 cm depth (topsoil + subsoil) and the rocky layer was absent. Soil texture was 35% sand and 35% clay and constant throughout the profile. Rock fragment content was 20% in the topsoil and 40% in the subsoil and bulk density was 1.5 kg/L. The corresponding soil water retention capacity was 216 mm. Macroporosity was 7% for both the topsoil and subsoil. Soil evaporation parameters were $\gamma = 0.5$ and $\kappa = 0.05$.

Vegetation – Two plant cohorts were considered, each of 10 m height, *D50* = 200 mm, *D95* = 800 mm and 40% cover. Ψ_{sp} = -2.0MPa, LAI_{sp} = 1.6 $m^2 \cdot m^{-2}$, k_{sp} = 0.5 and s_{sp} = 0.5 $mm \cdot LAI^{-1}$.

We evaluated the effect of modifying the following model parameters (Table S2.1): Leaf area of the cohort per area of the stand (*LAI*); rooting depth (*D50* and *D95* altered simultaneously); species-specific canopy storage capacity per LAI unit (s_{sp}); soil depth of layers 1-2 (d); annual rainfall (P_{ann}); shape and scale parameters of the gamma distribution for daily rainfall; and soil texture (from clayey soils to sandy soils); soil water potential corresponding to a 50% loss of whole-plant relative conductance (Ψ_{sp}). Each of those parameters decreased or increased by a fixed percentage (-80%, -40%, -20%, -10%, 0, +10%, +20%, +40%, +80%) and the remaining parameters were held constant.

Table. S3.1: Range of values considered for each studied parameter.

Parameter	Symbol	Units	Initial	Min (-80%)	Max (+80%)
Leaf area index (x2 cohorts)	*LAI*	$m^2 \cdot m^{-2}$	1.6	0.32	2.88
Rooting depth	*D50/D95*	mm	200/800	40/120	360/1440
Soil depth [water retention]	d	cm [mm H_2O]	100 [216]	20 [52]	180 [373]
Soil texture (clay/silt/sand)		%	35/30/35	63/30/7	7/30/63
Canopy storage capacity	s_{sp}	$mm \cdot LAI^{-1}$	0.5	0.1	0.9
Annual rainfall	P_{ann}	mm	622	124	1119
Gamma shape			2	0.4	3.6
Gamma scale			4	0.8	7.4
Potential corresponding to 50% conductance loss	Ψ_{sp}	MPa	-2.0	-0.4	-3.6

S2.2 Results

Sensitivity analyses were run to determine the effect of parameter changes on annual plant transpiration (Fig. S2.1b), drought intensity (Fig. S2.1c) and drought duration (Fig. S2.1d). As expected, the most influential variable was annual rainfall. An increase in annual rainfall lead to higher transpiration as well as milder and shorter drought. Drought stress was moderately sensitive to the shape and scale parameters of the Gamma distribution used to generate daily rainfall. Most importantly, very low values of shape or scale made the rainfall distribution become concentrated around small daily rainfall amounts (hence, more days of rain). In turn, this increased canopy interception and hence increased drought intensity and duration.

LAI was also a highly influential factor. Low LAI values imply low plant transpiration rates and this, despite the increase in soil evaporation, leads to lower drought stress. Very high LAI values may also decrease transpiration, because of the higher rainfall interception loss. Drought intensity and duration increase with LAI. Transpiration decreased and drought stress increased for shallow roots and shallow soils, due to larger water amounts being lost in those situations as runoff or deep drainage. Deep rooting and deep soils also increased transpiration, and decreased drought stress.

The sensitivity of drought stress to changes in canopy storage capacity was small compared to other parameters, although transpiration decreased and drought intensity and duration increased for large values of s_{sp} (and the reverse happened for small values). Soil texture had only a minor influence on drought stress, although sandy soils led to higher drought intensity values compared to more clayey soils. Finally, soil water potential corresponding to 50% loss in conductance affected plant transpiration, but appeared as relatively unimportant for drought stress compared to other factors. Note that the two plant cohorts had the same Ψ_{sp} values. Additional model simulations where plant cohorts differ in Ψ_{sp} values led to the cohort with lower Ψ_{sp} suffering higher stress (not shown).

Fig. S2.1: Climatic input (a) and results (b-d) of the sensitivity analyses.

a) Monthly temperature and rainfall

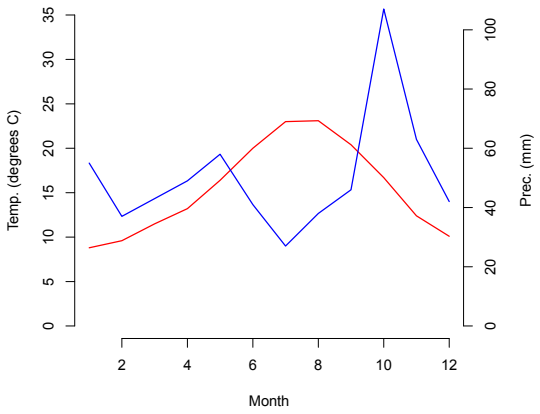

b) Plant transpiration

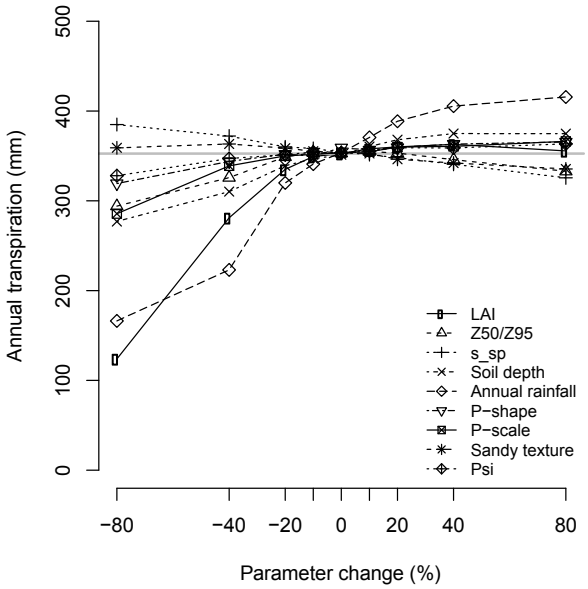

c) Drought intensity

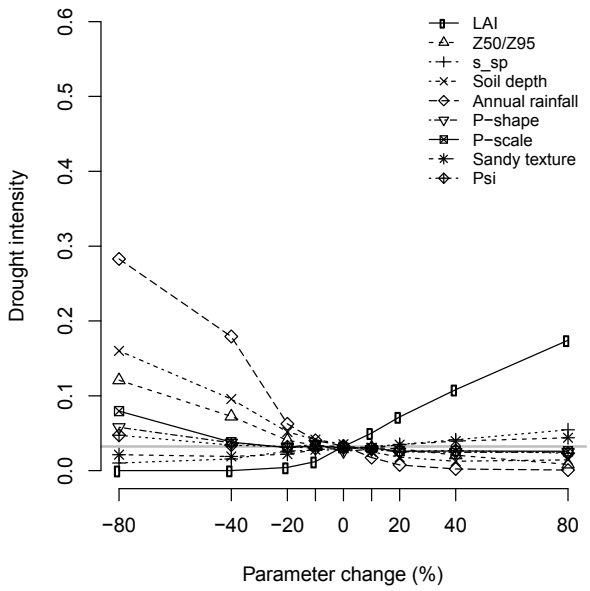

d) Drought duration

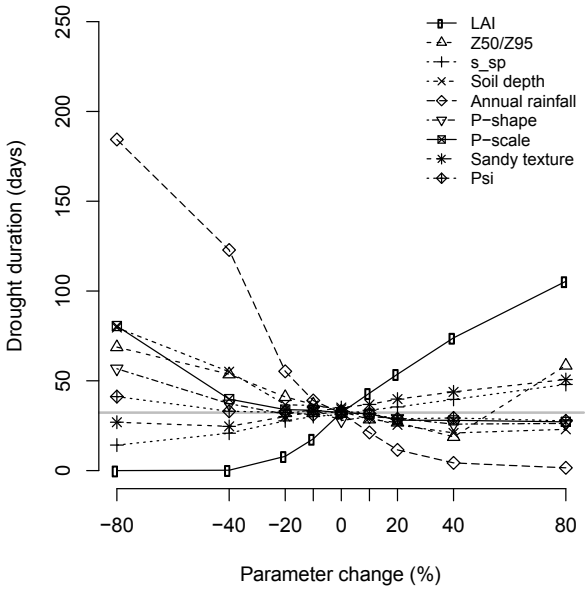

Appendix S3. Details of the calibration of species-specific parameters

Table S3.1 – Functional group classification

Functional group	Species included
Other trees	*Acer campestre, Acer opalus*, *Alnus glutinosa*, *Betula spp., Castanea sativa, Corylus avellana, Fraxinus spp., Quercus petraea, Quercus pyrenaica, Quercus robur, Sorbus aria, Sorbus aucuparia*
Shrub R+S– (resprouter)	*Arctostaphylos uva-ursi, Arbutus unedo*, *Asparagus spp.*, *Bupleurum fruticosum, Buxus sempervirens, Calluna vulgaris, Ceratonia siliqua, Chamaerops humilis, Clematis spp., Crataegus spp., Daphne spp., Globularia alypum, Ilex aquifolium, Juniperus communis, Juniperus oxycedrus, Laurus nobilis, Ligustrum vulgare, Lonicera spp., Olea europaea, Phillyrea spp., Pistacia lentiscus, Quercus coccifera, Rhamnus spp., Rubus spp., Rosa spp., Smilax aspera, Thymelaea spp. (tinctoria), Viburnum tinus.*
Shrub R–S+ (seeder)	*Bupleurum fruticescens, Cistus spp., Helianthemum spp., Lavandula spp., Rosmarinus officinalis, Ulex parviflorus*
Shrub R+S+ (resprouter/seeder)	*Calicotome spinosa, Colutea arborescens, Coronilla spp., Cytisus spp., Dorycnium spp., Erica arborea, Erica scoparia*, *Erica multiflora, Genista spp., Halimium spp., Ononis spp., Spartium junceum, Thymus spp. (vulgaris)*

Table S3.2 – Calibration of canopy storage capacity per LAI unit (s_{sp}): Watanabe & Mizutani (1996) suggested that the ratio between canopy water storage capacity (S) and LAI was S/LAI = 0.15 mm for broadleaved forests and S/LAI = 0.2 mm for coniferous stands, although higher values have been reported. Using bibliographic sources we compiled data regarding S and LAI measurements made on the same (or very similar) stands (or plants) (Table S4.2). The resulting S/LAI ratios may vary substantially from one stand to the other (e.g., *Pinus sylvestris*). We decreased the precision of s_{sp} values, making them equal for many species, to account for the lack of accuracy of S/LAI estimates.

Species/functional group	**Reference**	**S** (mm)	**LAI** ($m^2 \cdot m^{-2}$)	**S/LAI** (mm/LAI^{-1})	s_{sp} (mm/LAI^{-1})
Pinus halepensis	Molina & Del Campo (2012)	3.6	2.6	1.385	**1.00**
Pinus nigra	Robins (1974)	1.0	-	-	**1.00**
Pinus sylvestris	Llorens & Gallart (2000)	1.96	1.1	1.815	**1.00**
	Llorens (1997), Poyatos et al. (2007)	1.34	2.4	0.558	
Pinus uncinata	-	-	-	-	**1.00**
Pinus pinea	-	-	-	-	**1.00**
Pinus pinaster	Loustau et al. (1992)	0.52	3.0	0.173	**1.00**
Abies alba					
Quercus ilex	Limousin et al. (2008)	2.60	3.14	0.82	**0.50**
Quercus suber					**0.50**
Quercus humilis	Muzylo et al. (2009)	0.49	3.35	0.146	**0.50**
Quercus faginea					**0.50**
Fagus sylvatica	Proisy et al. (2000)	0.73	6.7	0.109	**0.25**
Other trees *Carpinus*+*Q.humilis*+other	Sraj et al. (2008)	1.25	5.7	0.219	**0.25**
Shrub R+S-	-	-	-	-	**0.25**
Shrub R-S+ *Rosmarinus officinalis*	García-Estrigana et al. (2010)	1.20	2.8	0.42	**0.25**
Shrub R+S+ *Dorycnium pentaphyllum*	García-Estrigana et al. (2010)	0.77	1.5	0.51	**0.25**

Table S3.3 - Calibration of critical water potentials: Calibration of Ψ_{sp} according to different sources of information (all values are in MPa). Ψ_{min} – Minimum recorded leaf water potentials (Choat et al., 2012; Martínez-Vilalta et al., 2014); $\Psi_{50\ plc}$ and $\Psi_{88\ plc}$ – Water potentials causing 50% and 88% xylem embolism in stems (Choat et al. 2012); Ψ_{tlp} – Water potential at turgor loss point (Bartlett et al., 2012); Ψ_{50gs} – Water potential at 50% stomatal closure (Klein, 2014). Recent investigations indicate that $\Psi_{50\ plc}$ measurements may have been overestimated (e.g., Delzon & Cochard 2014; Martin-StPaul et al., 2014), which means that more negative Ψ_{sp} values could be adopted for some species (particularly for species with long xylem vessels such as *Quercus* spp.).

Species/functional group	Ψ_{min}	Ψ_{50plc}	Ψ_{88plc}	Ψ_{tlp}	Ψ_{50gs}	Ψ_{sp}
Pinus halepensis	-2.60	-3.11	-5.16	–	-1.40	**-2.0**
Pinus nigra	-2.40	-2.80	-3.70	–	–	**-2.0**
Pinus sylvestris	-2.28	-3.61	-5.70	–	-2.15	**-2.0**
Pinus uncinata	–	-4.18	–	–	–	**-2.0**
Pinus pinea	-2.40	-3.65	-6.42	–	–	**-2.0**
Pinus pinaster	-2.00	-3.01	-4.45	–	–	**-2.0**
Abies alba	-4.00	-3.65	-4.40	–	-2.00	**-2.0**
Quercus ilex	-4.07	-2.02	-4.17	-2.84	-3.05	**-3.0**
Quercus suber	–	–	–	-3.08	-2.90	**-3.0**
Quercus humilis	-4.60	-3.30	-5.50	–	-3.80	**-3.0**
Quercus faginea	–	–	–	-2.67	-3.65	**-3.0**
Fagus sylvatica	-2.37	-3.20	-3.80	-2.17	-2.15	**-2.0**
Other trees						**-2.0**
Acer campestre	–	-2.00	–	–	-1.90	
Shrub R+S-						**-4.0**
Quercus coccifera	–	-6.96	–	-2.95	-2.30	
Arbutus unedo	-3.03	-3.09	-4.84	-0.98	–	
Buxus sempervirens	–	-8.00	–	–	–	
Juniperus communis	–	-6.43	-7.72	–	–	
Ligustrum vulgare	–	-2.82	–	–	–	
Ceratonia siliqua	–	-8.12	–	-1.82	-1.90	
Shrub R-S+						**-5.0**
Cistus albidus	-6.18	-5.78	-8.86	–	–	
Ulex europaeus	–	-6.58	–	–	–	
Shrub R+S+						
Erica arborea	–	-2.70	-4.60	–	–	**-3.0**

Fig. S3.1 – Calibration of the relationship between basal area and leaf area index: Scatter diagrams and linear regressions with zero intercept between basal area and leaf area index (LAI) of different species, using data from Burriel et al. (2004). LAI values were obtained dividing leaf biomass by specific leaf mass. Leaf biomass was, in turn, estimated using allometric relationships between branch diameter and leaf dry mass and the distribution of the number of branches of each branch diameter class, the latter being measured in one tree per diameter class of the forest plot (details in Burriel et al. 2004).

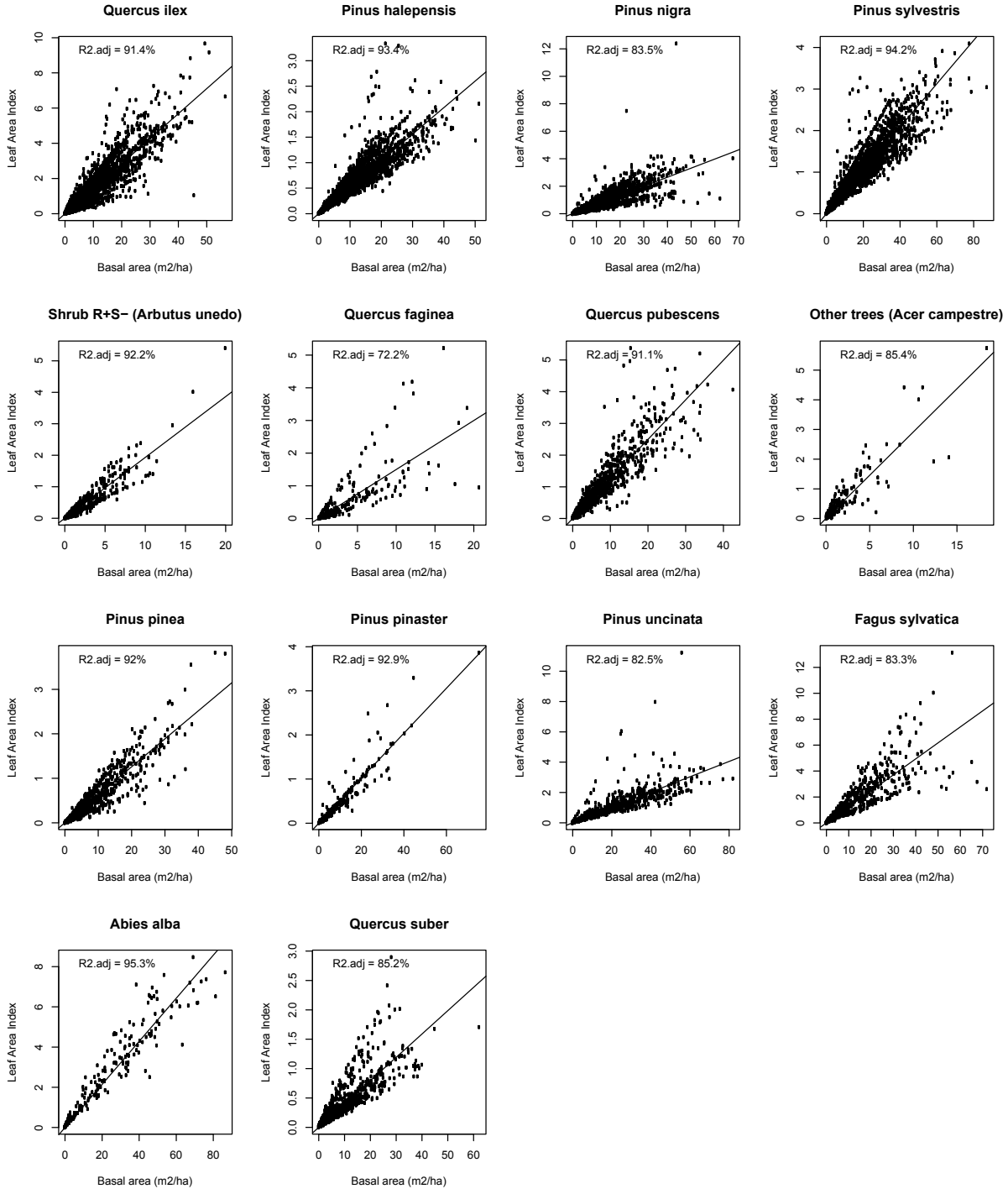

Bibliography

Bartlett, M.K., Scoffoni, C., Sack, L., 2012. The determinants of leaf turgor loss point and prediction of drought tolerance of species and biomes: a global meta-analysis. Ecol. Lett. 15, 393–405. doi:10.1111/j.1461-0248.2012.01751.x

Burriel, J.A., Gracia, C., Ibàñez, J.J., Mata, T., Vayreda, J., 2004. Inventari Ecològic i Forestal de Catalunya, Mètodes. CREAF, Bellaterra, Spain.

Choat, B., Jansen, S., Brodribb, T.J., Cochard, H., Delzon, S., Bhaskar, R., Bucci, S.J., Feild, T.S., Gleason, S.M., Hacke, U.G., Jacobsen, A.L., Lens, F., Maherali, H., Martínez-Vilalta, J., Mayr, S., Mencuccini, M., Mitchell, P.J., Nardini, A., Pittermann, J., Pratt, R.B., Sperry, J.S., Westoby, M., Wright, I.J., Zanne, A.E., 2012. Global convergence in the vulnerability of forests to drought. Nature 491, 752–755. doi:10.1038/nature11688

Delzon, S., Cochard, H., 2014. Recent advances in tree hydraulics highlight the ecological significance of the hydraulic safety margin. New Phytol. 203, 355–358. doi:10.1111/nph.12798

Garcia-Estringana, P., Alonso-Blázquez, N., Alegre, J., 2010. Water storage capacity, stemflow and water funneling in Mediterranean shrubs. J. Hydrol. 389, 363–372. doi:10.1016/j.jhydrol.2010.06.017

Klein, T., 2014. The variability of stomatal sensitivity to leaf water potential across tree species indicates a continuum between isohydric and anisohydric behaviours. Funct. Ecol. 28, 1313–1320. doi:10.1111/1365-2435.12289

Limousin, J.-M., Rambal, S., Ourcival, J.-M., Joffre, R., 2008. Modelling rainfall interception in a mediterranean Quercus ilex ecosystem: Lesson from a throughfall exclusion experiment. J. Hydrol. 357, 57–66. doi:10.1016/j.jhydrol.2008.05.001

Llorens, P., 1997. Rainfall interception by a Pinus sylvestris forest patch overgrown in a Mediterranean mountainous abandoned area .2. Assessment of the applicability of Gash's analytical model. J. Hydrol. 199, 346–359.

Llorens, P., Gallart, F., 2000. A simplified method for forest water storage capacity measurement. J. Hydrol. 240, 131–144.

Loustau, D., Berbigier, P., Granier, A., Moussa, F., 1992. Interception loss, throughfall and stemflow in a maritime pine stand. I. Variability of throughfall and stemflow beneath the pine canopy. J. Hydrol. 138, 449–467.

Martin-StPaul, N.K., Longepierre, D., Huc, R., Delzon, S., Burlett, R., Joffre, R., Rambal, S., Cochard, H., 2014. How reliable are methods to assess xylem vulnerability to cavitation? The issue of "open vessel" artifact in oaks. Tree Physiol. 1–12. doi:10.1093/treephys/tpu059

Martínez-Vilalta, J., Poyatos, R., Aguadé, D., Retana, J., Mencuccini, M., 2014. A new look at water transport regulation in plants. New Phytol. doi:10.1111/nph.12912

Molina, A.J., del Campo, A.D., 2012. The effects of experimental thinning on throughfall and stemflow: A contribution towards hydrology-oriented silviculture in Aleppo pine plantations. For. Ecol. Manage. 269, 206–213. doi:10.1016/j.foreco.2011.12.037

Muzylo, A., Llorens, P., Valente, F., Keizer, J.J., Domingo, F., Gash, J.H.C., 2009. A review of rainfall interception modelling. J. Hydrol. 370, 191–206. doi:10.1016/j.jhydrol.2009.02.058

Poyatos, R., Villagarcía, L., Domingo, F., Piñol, J., Llorens, P., 2007. Modelling evapotranspiration in a Scots pine stand under Mediterranean mountain climate using the GLUE methodology. Agric. For. Meteorol. 146, 13–28. doi:10.1016/j.agrformet.2007.05.003

Proisy, C., Mougin, E., 2000. Monitoring seasonal changes of a mixed temperate forest using ERS SAR observations. IEEE Trans. Geosci. Remote Sens. 38, 540–552.

Robins, P.C., 1974. A method of measuring the aerodynamic resistance to the transport of water vapour from forest canopies. J. Appl. Ecol. 315–325.

Šraj, M., Brilly, M., Mikoš, M., 2008. Rainfall interception by two deciduous Mediterranean forests of contrasting stature in Slovenia. Agric. For. Meteorol. 148, 121–134.

Watanabe, T., Mizutani, K., 1996. Model study on micrometeorological aspects of rainfall interception over an evergreen broad-leaved. Agric. For. Meteorol. 80, 195–214.

Appendix S4. Supplementary figures

Fig. S4.1: Optimum root distribution for all species in all forest plots. Boxplots are shown for combinations of species, stand LAI (either < 1.5 or > 1.5), soil texture (F – fine; M/C – medium or coarse) and aridity index (AI), calculated as the ratio between annual rainfall and annual PET. N – Number of plots for each combination of rock fragment content and rainfall range.

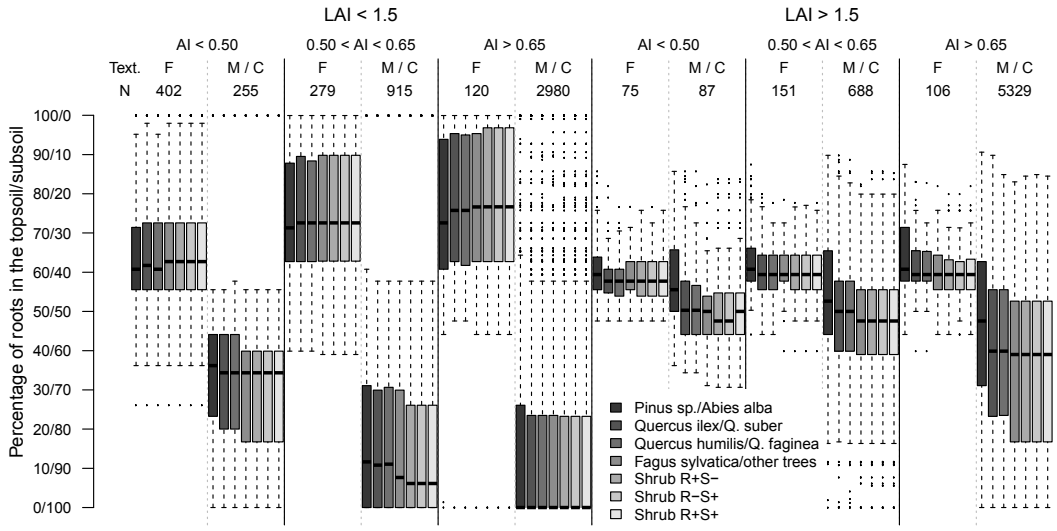

Fig. S4.2: Average drought stress for the 1980-2010 period (left panels) and change in drought stress (right panels). Boxplots show the stress values for plot records where the species was present in the SFI3.

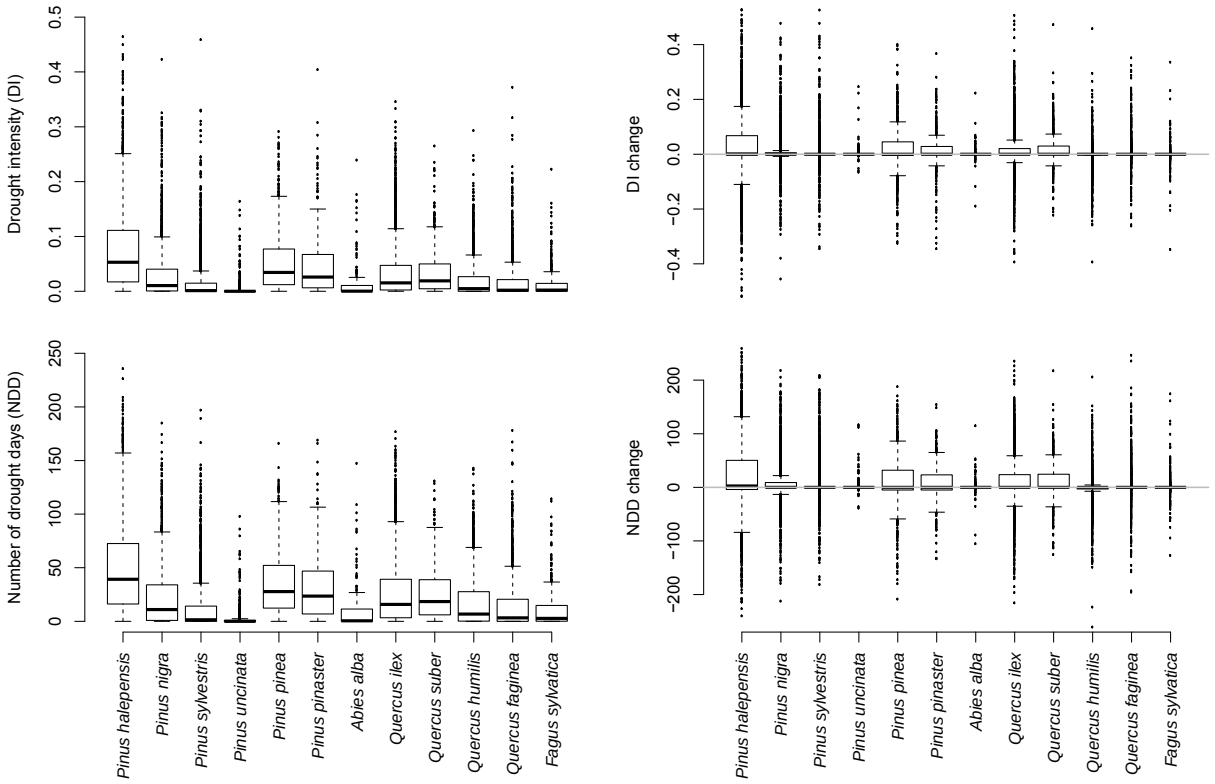

Fig. S4.3: Predicted average drought intensity (DI) for the 1980-2010 period.

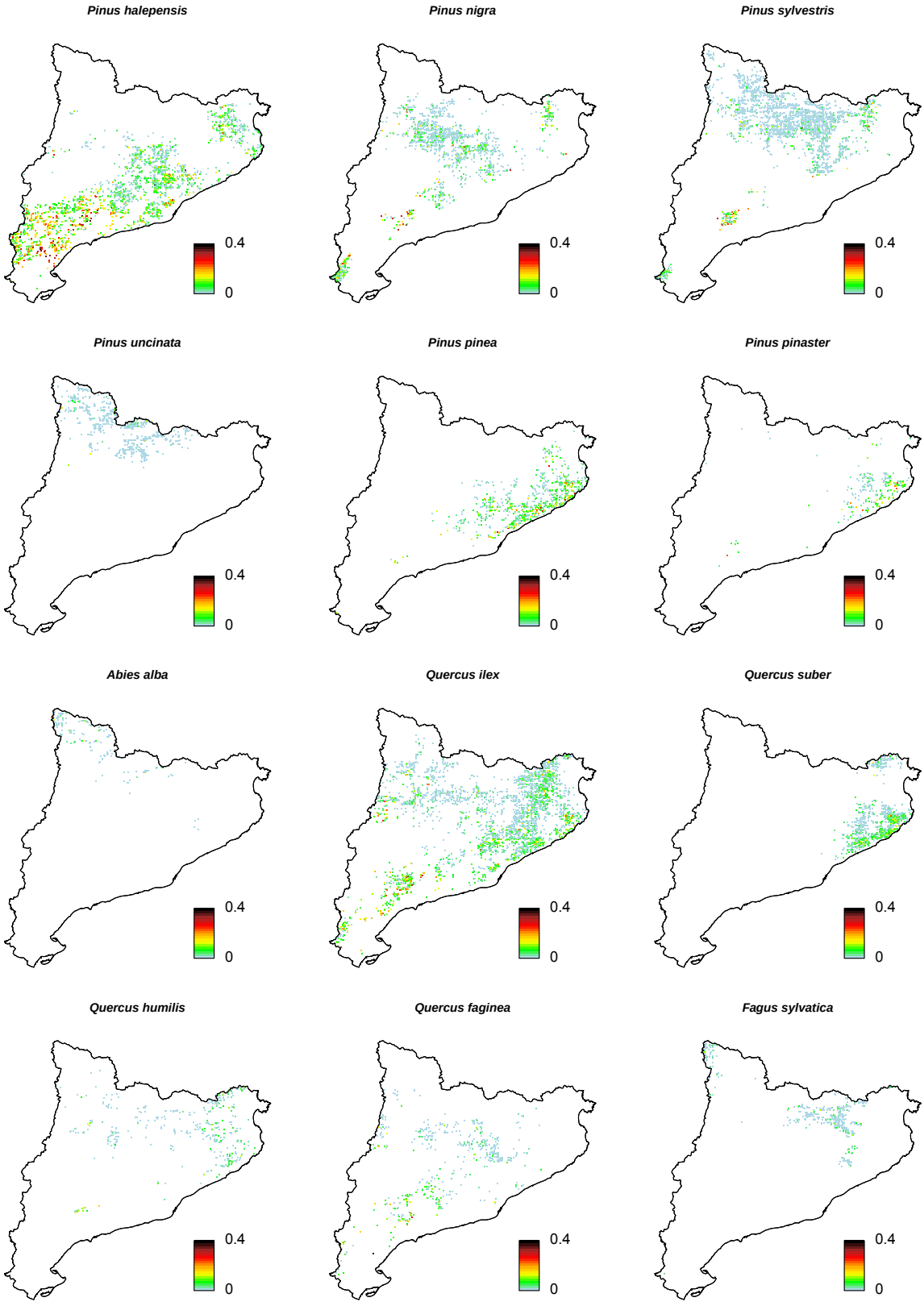

Fig. S4.4: Predicted average drought intensity (DI) for the 1980-2010 period, after relativizing with respect to the distribution of values for the species (i.e, values are percentiles of the distribution).

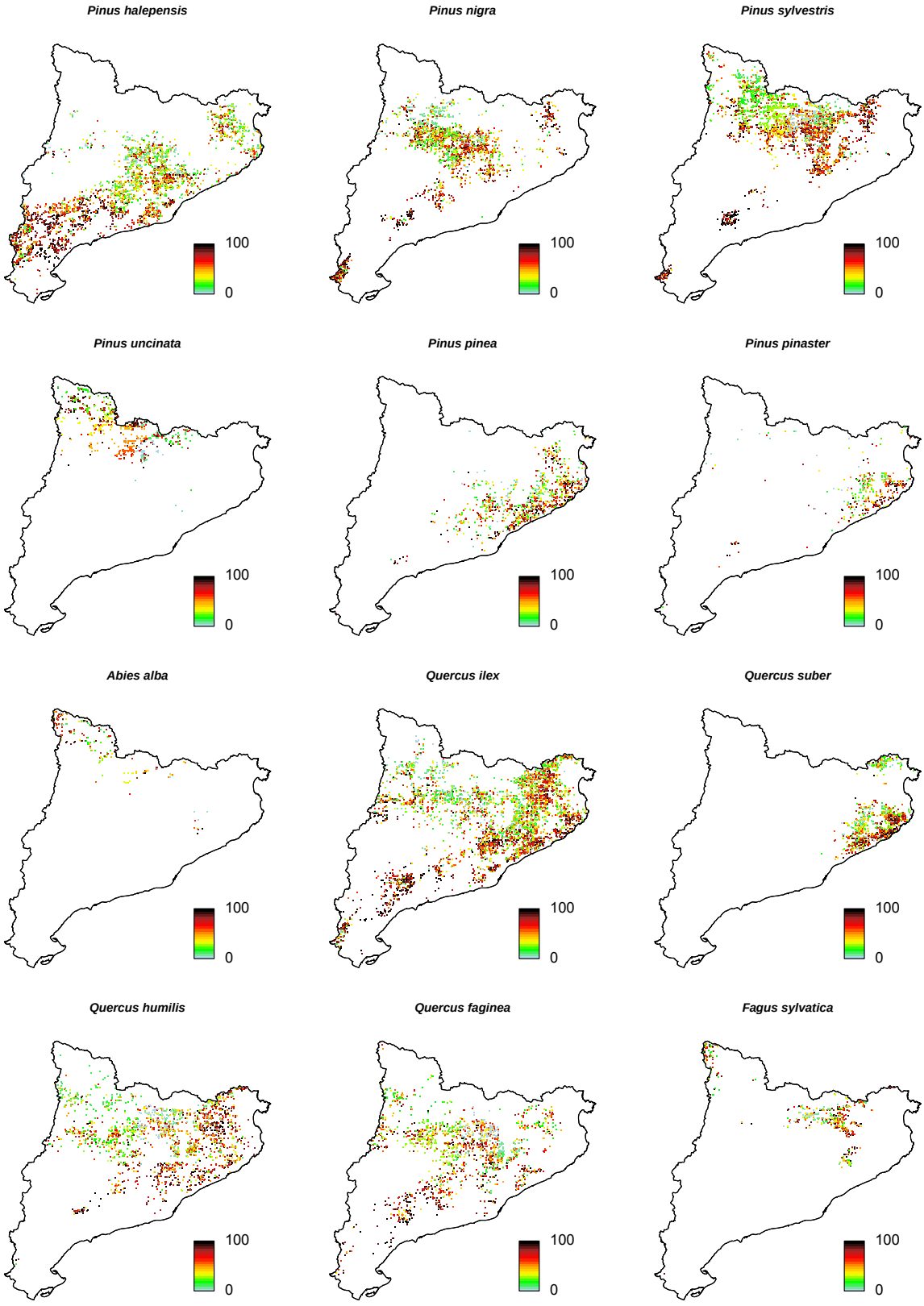

Fig. S4.5: Predicted average number of drought days (NDD) for the 1980-2010 period.

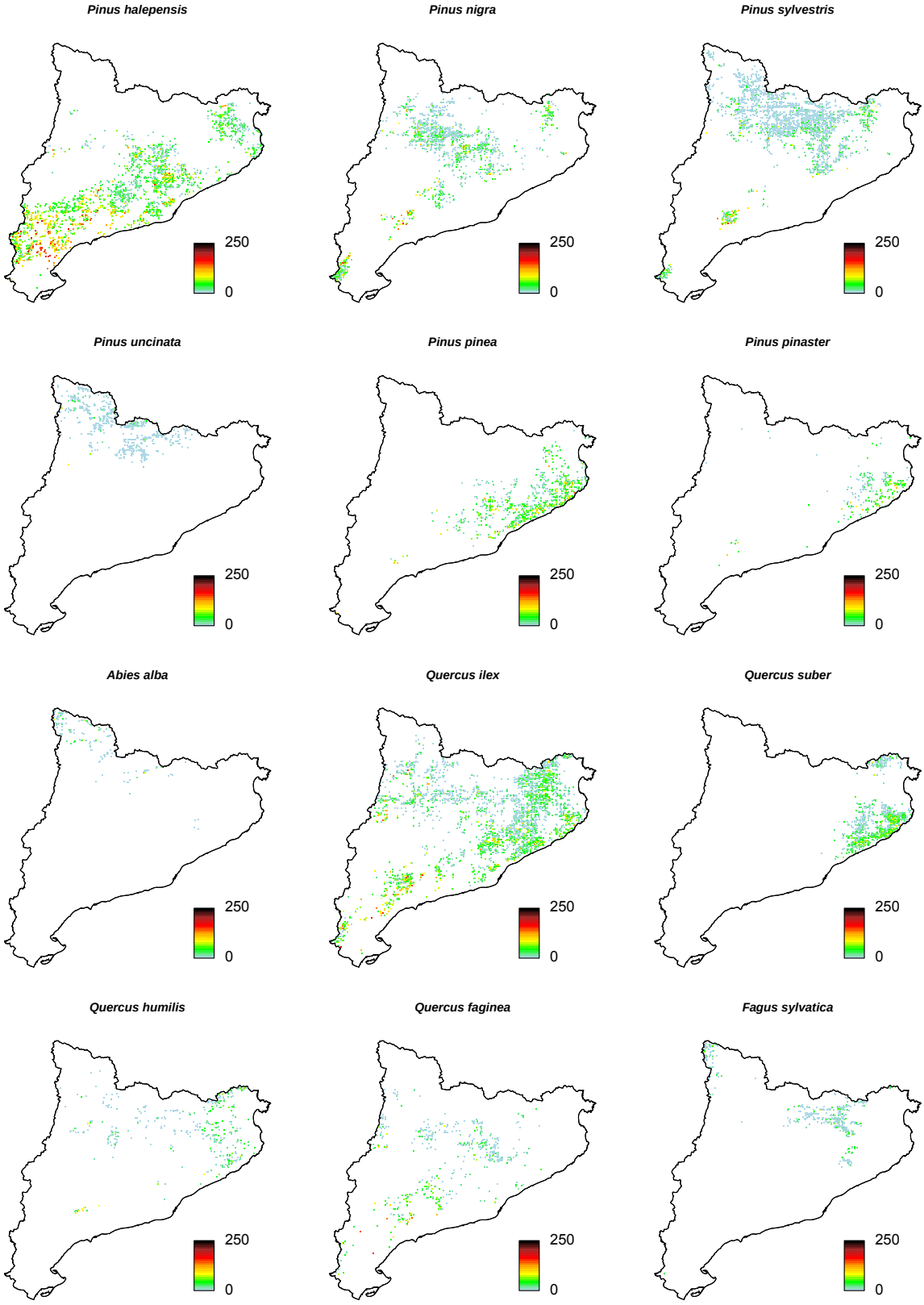

Fig. S4.6: Predicted average number of drought days (NDD) for the 1980-2010 period, after relativizing with respect to the distribution of values for the species (i.e, values are percentiles of the distribution).

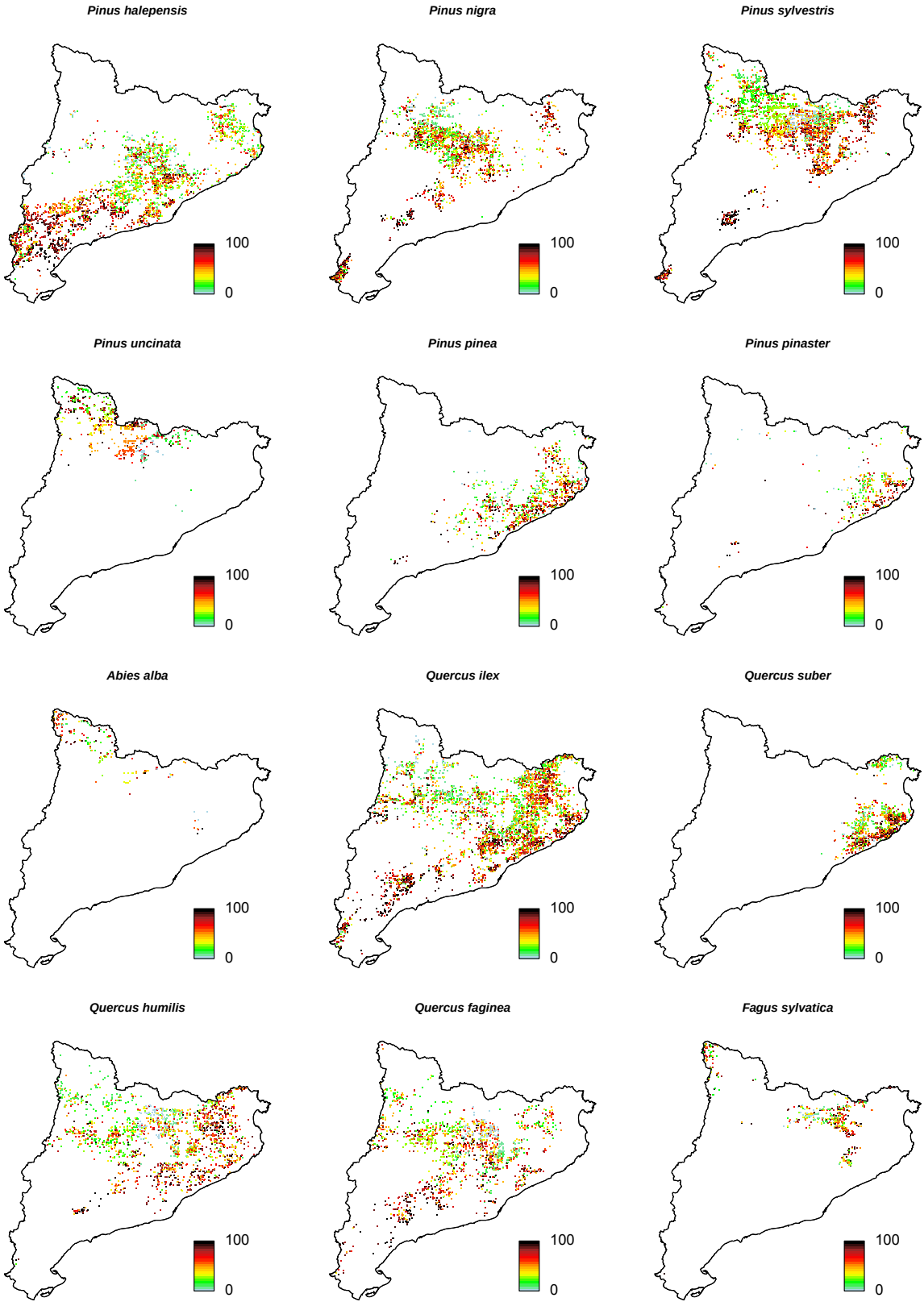

Fig. S4.6: Predicted change in drought intensity (DI) during the 1980-2010 period. Only statistically significant ($p < 0.05$) changes are shown.

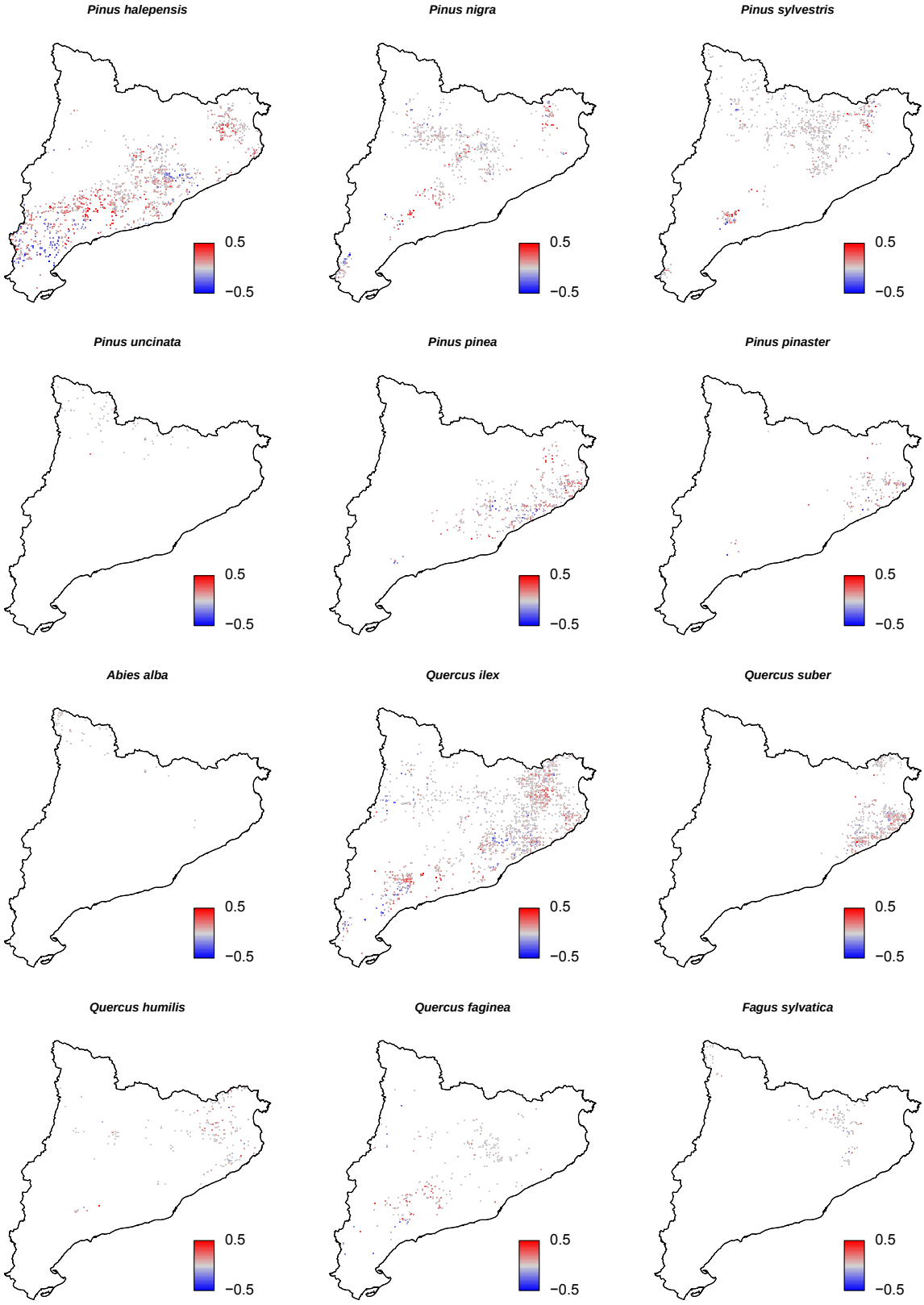

Fig. S4.7: Predicted change in number of drought days (NDD) during the 1980-2010 period. Only statistically significant ($p < 0.05$) changes are shown.